Quantitative Assessment of First-Party Risk in UAM Operations

Leonid Sedov[1)†], Valentin Polishchuk[1)], Mitsuki Tanoue[1)], Manuel Waltert[2)], and Xavier Olive[3)]

[1)]*Flight Logistics Unit, Communications and Transport Systems, Linköping University, Sweden*
[2)]*Centre for Aviation, Zurich University of Applied Sciences, Winterthur, Switzerland*
[3)]*ONERA DTIS, Université de Toulouse, Toulouse, France*
[†]*email: leonid.sedov@liu.se*

This paper explores first-party risk assessment for Urban Air Mobility (UAM) operations, focusing specifically on risks to the flying vehicle itself and its occupants. Unlike third-party risk, which concerns people and property on the ground, first-party risk directly affects operational safety and mission planning. We propose a demand-driven probabilistic framework for estimating the spatial distribution of UAM traffic, enabling the quantification of the likelihood of observing a UAM vehicle across different parts of a geographical region of interest (ROI). Building on this distribution, we introduce a methodology for estimating the Expected Fatality Rate (EFR) associated with a given UAM mission, accounting for mission-specific parameters and risk exposure levels. To demonstrate the feasibility of our approach, we present a proof-of-concept implementation of a graphical user interface (GUI) that integrates demand modeling with risk estimation, illustrating how the framework can be applied in practice. The results highlight the potential for more refined and operationally relevant safety metrics. Overall, this work establishes a foundation for first-party risk assessment in UAM, paving the way for more comprehensive, data-driven, and context-aware methodologies in future research.

Key Words : Unmanned Traffic Management, Urban Air Mobility, Safety, Risk assessment

1. Introduction

Unmanned Aerial Vehicles (UAVs) are entering the skies of our cities, calling for an introduction of the Unmanned Traffic Management (UTM) system to handle the potentially dense urban air traffic. Most attention in UTM has been drawn to operations by *small* drones (delivery, inspections, etc.). Such drones are relatively inexpensive, and their loss is insignificant compared to the hazards they may pose to manned aviation or to people on the ground. That is, UTM is mostly focused on estimating and mitigating *third-party risk*, i.e., the risk of a drone interfering with other airspace users or injuring the uninvolved population in the city.

Urban Air Mobility (UAM) is a novel concept which envisions the transportation of passengers through metropolitan airspace (the European Union Aviation Safety Agency – EASA – provides a comprehensive comparison of the differences between definitions of UAM by authorities in different countries [1]). For UAM operations, loss of hull is already an issue, similarly to conventional aviation; moreover, for passenger-carrying vehicles, the loss is a catastrophic event. In this paper, we analyze such *first-party risks* for people flying a UAM aircraft in urban airspace.

Risk assessment of urban airspace flights is usually divided into two task: ground risk and air risk estimation [2, 3], both of which belong to the third-party risk assessment. Many countries have adopted the Specific Operations Risk Assessment (SORA) [2] methodology as their default means of risk assessment for the operations of unmanned aerial systems (UAS). SORA focuses on UAVs that fall under the Specific category (hence the name), and is primarily a *qualitative* methodology in which the user goes through a decision tree based on the characteristics of both the aircraft and the mission to find the air and ground risk classes of the operation, which are then used to derive the Specific assurance and integrity level (SAIL). SORA also allows claiming risk reduction by providing quantitative proofs that the exposure of population or conventional aircraft to risk is smaller than SORA's conservative qualitative estimates: the EU-funded AiRMOUR project [4] recommends using historical flight data and population patterns to that end. Quantitative third-party risk analysis for UTM has been carried out in [5, 6, 7, 8]. In this paper, we study *quantitative* estimations of *first-party* risk.

1.1. Related work

Drone conflicts have been extensively studied as part of airspace capacity estimation in [9, 10, 11, 12, 13, 14]. These papers calculate the risk based on the flight's dwelling time in a given airspace and do not suggest ways for determining the risk from the aircraft precise trajectory, which precludes detailed analysis and fine-tuning of the flight plan.

La Cour Harbo and Schiøler [5] provide quantitative estimates of the air risk that a drone flight poses to conventional aviation by calculating the expected rates of vertical and horizontal conflicts based on historical flight data. They argue that drones primarily pose a threat to General Aviation (GA), as such aircraft are more likely to enter the airspace at altitudes where drones operate (below 100 m). The authors further quantify the probability of GA aircraft going to the altitude below 100 m, which, although generally not permitted, still occurs due to factors such as emergencies, pilot errors, intentional violations, etc.

However, the methodology proposed in [5] is not well suited for fine-tuning individual missions, as it relies on aggregated traffic density statistics over larger spatial areas and extended time periods (e.g., weeks or months). To address this limitation, Olive et al. [6] developed a high-fidelity quantitative methodology that uses historical GA flight tracks to construct a fine-grained map of the probability of observing GA aircraft in different places in the region of interest (ROI); this probability map is then used to assess a particular drone mission, enabling detailed analysis of where exactly along the route the risk is highest, as well as how it varies at different times of day and days of the week.

Similarly to [6], we construct a probabilistic map which shows the expected number of drones in different parts of a ROI. Our approach is inspired by the *Likely UTM (LiU) map* proposed in [9] and is based on estimating UAM demand and analyzing where vehicles serving this demand are more likely to operate. We use this map to calculate the expected conflict rate for a given mission (that is, how often the given mission is expected to lose separation from other airspace users and has to deconflict). This conflict rate is subsequently used to estimate the Expected Fatality Rate (EFR) of the mission.

Calculations of our variant of the *LiU-map* are closely related to the concept of betweenness centrality in graph theory [15], which quantifies the number of paths passing through a given vertex. The continuous analogue of betweenness centrality remains largely unexplored; to the best of our knowledge, the only related work is [16], which derives the distribution of chords intersecting different points in the unit disk as a function of distance from the disk center.

1.2. Contributions and roadmap

First-party risks have long been studied in conventional aviation. In this paper, we consider them for a UAM-related application. Differently from earlier work which assessed third-party risks *from* a specific vehicle *to* other vehicles and people, we estimate the risk that *other* urban aircraft impose *on* a given planned UAM mission (such as drone taxi operations, where the lives of passengers on the vehicle are at danger in case of a conflict with another flying vehicle). Similarly to earlier work, we use *quantitative* methodology but apply it to the new domain of UAM.

Specifically, Section 2 describes how the probabilistic convex hull-based *Likely UTM (LiU) map* is computed. In Section 3, we sketch the methodology for estimating first-party risk, given a mission plan and a pre-computed *LiU map*. Section 4 presents our interactive web tool prototype for first-party risk assessment along with a case-study of a railway inspection mission. We conclude in Section 5 and discuss directions for future work.

The topic of quantitative risk assessment of UAM operations is of special interest to both the scientific community and industry stakeholders. Commissioned by the ICAO, a review by the UAM working group of the International Forum for Aviation Research (IFAR) [17] provides an analysis of the current state and future research needs for UAM and, in particular, emphasizes the need for comprehensive risk assessment frameworks.

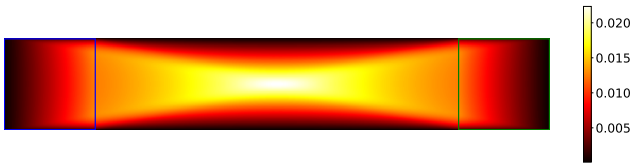

Fig. 1. Example of route density between the blue and the green squares (left and right, respectively). The figure is discretized into a 600×100 grid, with each square occupying pixels (the left and the right squares are 100×100 pixels each) and took all segments connecting pixels in the left square to those in the right square; the resulting heatmap shows the proportion of routes passing through each pixel. Although the utilization at the most congested central point is more than seven times higher than at the least utilized boundary regions, for most of the domain the deviation from the central value remains within a factor of two.

2. The convex hull-based LiU map

Ideally, for a proper risk estimation, precise historical data on flight tracks of UAM vehicles in cities would be desired. Unfortunately, such data is currently available in very few locations worldwide. In the absence of this data, we propose constructing a probabilistic map that represents the likelihood of observing drone operations across the city based on estimated demand.

The idea for a similar map was previously explored in [9], which used a very detailed discretized population density map as input. In this paper, we adapt the methodology from [9] to the case in which the population density is given as a set P of polygons, with each polygon $a \in P$ assigned a weight $D(a)$ corresponding to the number of people in the polygon.

We assume a simplified model in which all drones operate at the same speed and at the same altitude, and the demand for UAM operations (departure or arrival) in each polygon $a \in P$ is proportional to the number of people, $D(a)$, living there. Since our methodology depends only on the relative distribution of demand across polygons, it can readily be extended to more sophisticated demand models.[1].

We go through every pair $a, b \in P$ of polygons and compute their convex hull $CH(a, b)$, which represents the envelope of all possible straight-line flights between the polygons. We assume that flights between a and b are uniformly distributed within the convex hull, i.e., the density of a-b routes is constant over $CH(a, b)$ – this suffices for practical purposes (Fig. 1).[2]

We discretize the ROI into a grid S of square pixels and compute, for each pixel, the probability of observing a drone.

[1] More detailed and elaborate approaches may incorporate socioeconomic characteristics of the population in each polygon (e.g., age or income) or account for additional demand sources not tied to population density, such as commercial centers or delivery hubs. As the focus of this paper is on risk estimation rather than demand modeling, we limit ourselves to population-based demand.

[2] Non-uniform route distributions can readily be incorporated into our model.

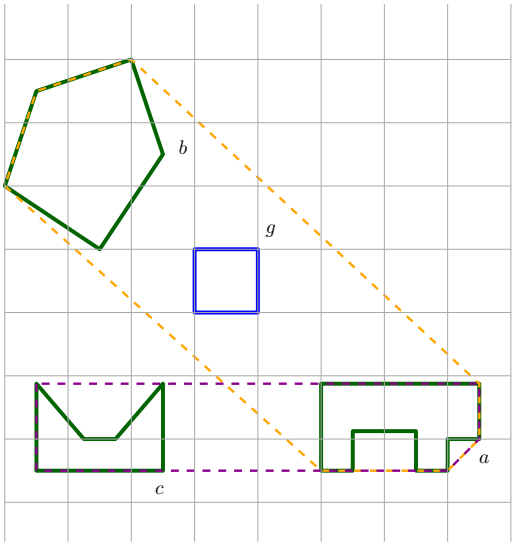

Fig. 2. The convex hull of polygons $a, b \in P$ (orange dashed line) intersects pixel g and therefore contributes $D(a)D(b)$ to the probability of observing a drone in g. In contrast, $CH(a, c)$ (purple dashed line) does not intersect g, so it does not contribute to the probability of seeing a drone in g.

Specifically, for a pixel $g \in S$ let

$$I_s = \{(a, b) \in P \times P | g \cap CH(a, b) \neq \emptyset\} \tag{1}$$

denote the set of all pairs (a, b) of polygons from P whose convex hull $CH(a, b)$ intersects g – operations between a and b may overfly pixel g, contributing to the first-party risk in that location (Fig. 2). Notwithstanding abuse of notation, we use $|\cdot|$ to denote the area of a set in the plane. Then let $R_g(a, b) = \frac{|CH(a,b) \cap g|}{|g|}$ be the fraction of the area of g intersected by the convex hull $CH(a, b)$ – if the convex hull only partially overlaps with the pixel, the contribution of routes between a and b to the first-party risk in g is correspondingly reduced.

We call the function

$$m(g) = \sum_{(a,b) \in I_g} R_g(a, b) D(a) D(b) \tag{2}$$

the *Likely UTM (LiU) map*; this map represents the relative likelihood of observing a drone above pixel g. If exactly one drone is present in the ROI, then the probability that the drone is in g is

$$\frac{m(g)}{\sum_{s \in S} m(s)} \tag{3}$$

Let N denote the expected number of drones that are simultaneously in the air in the ROI[3]. The expected number of drones above pixel g at any given time is then

$$E(g) = N \frac{m(g)}{\sum_{s \in S} m(s)}. \tag{4}$$

[3]Assuming that the intensity of drone flights is uniform over the day (e.g., $\tau = 12hrs$), a rough estimate of N is $N = N_{tot} t / \tau$ where N_{tot} is the total number of drone operations expected during this period and t is the average duration of a flight; more precise estimations (outside the scope of this paper) can be obtained from a distribution of flights over the day.

3. First-party risk estimation methodology

We build upon the convex-hull-based *LiU map*, described in the previous section, to develop a high-fidelity methodology for estimating first-party risk for a given UAM mission. Our approach is inspired by the air risk estimation methodology proposed in [6], which in turn builds upon [5] which focused on the interaction between GA and drones. Specifically, in [5] the aircraft (both drones and GA) are represented as cylinders, and the Mid-Air Collision (MAC) rate is defined as

$$p_{\text{MAC}} = p_{\text{HC}} \cdot p_{\text{VC}} \cdot p_{\text{below}} \cdot \lambda_{\text{STM}} \tag{5}$$

where p_{HC} denotes the horizontal conflict rate (i.e., the rate with which the cylinder of a given aircraft will be intersected by other cylinders), p_{VC} is the probability of a vertical conflict, p_{below} is the probability of a GA aircraft going below the minimum allowed altitude, and λ_{STM} is the factor representing tactical and strategic deconfliction capabilities of both the own vehicle (for which the risk is being estimated) and the GA aircraft.

In this paper, we focus on UAM–UAM interaction (i.e., UAM aircraft to UAM aircraft conflicts). Urban air operations are generally confined to low level airspace, typically below 150 m. Due to the need to minimize noise and visual pollution and to avoid damaging property on the ground, it is beneficial for UAM aircraft to operate as high as possible within this limited airspace. This means that UAM operations will occupy a thin altitude band[4], implying that there may not be much space for vertical deconfliction. In our model, we assume that UAM aircraft operate at approximately the same altitude and set $p_{\text{VC}} = 1$. Consequently, in this case the term p_{below} becomes redundant and is also set to 1. More complex airspace structures, such as the layered airspace concept introduced in [10] and further studied in [12, 11], can be included in the model by treating aircraft from different layers (altitude levels) separately – the total expected MAC rate is then the sum of the MAC expectations over the aircraft in the different layers.

We estimate the horizontal conflict rate using the *LiU map* introduced in Section 2. Specifically, the input to our method is the ground track of a UAM mission, denoted by ℓ. Let $2r$ be the minimum separation requirement, i.e., r is the safety radius around an urban aircraft. We "fatten" ℓ by r (i.e., compute the Minkowski sum of ℓ and radius-r disk) and denote the fattened path by L. This region represents all positions of other aircraft that would violate the separation requirement with a vehicle following ℓ. We then identify the set of pixels $S^* = \{g \in S \mid g \cap L \neq \emptyset\}$ intersected by L. Any drone located within these pixels may create a risk of mid-air collision (MAC) for a UAM aircraft operating along ℓ. We assume that the distribution of drones within each

[4]To quote EASA's UAM FAQ [18], "delivery drones with an average wingspan of 3 m and air taxis with an average wingspan of 12 m, [are] all flying at an average altitude of 150 m".

pixel $g \in S^*$ is uniform (following the same reasoning as in Section 2). Therefore, the expected number of drones in g that may conflict with the UAM aircraft is proportional to the area of g covered by L, i.e., to $|g \cap L|$. The total expected number of drones within L at any given moment of time is then

$$T = \sum_{g \in S^*} \frac{|L \cap g|}{|g|} E(g), \tag{6}$$

where $|\cdot|$ denotes the area and $E(g)$ is the expected number of drones in g – see Formula 4.

Following the same reasoning as in [5, 6], we define the MAC rate in the horizontal plane as

$$p_{\mathrm{HC}} = \frac{2r^2 T \sqrt{v_{\mathrm{OV}}^2 + v_{\mathrm{UA}}^2}}{r|L|}, \tag{7}$$

where v_{OV} and v_{UA} are the average speeds of the own vehicle and other aircraft, respectively. Similarly to how Arctic Science RPAS Operator's Handbook [19] and Weibel and Hansman [20] defined the expected fatality rate (EFR) created by 3rd-party air risk (i.e., risk imposed by own vehicle to conventional aviation), we define the first-party EFR of the UAM mission to be

$$\mathrm{EFR} = p_{\mathrm{MAC}} \cdot n \cdot p\{\text{loss of aircraft}|\mathrm{MAC}\} \tag{8}$$

where n is the number of occupants in the UAM vehicle for which first-party risk is computed and $p\{\text{loss of aircraft}|\mathrm{MAC}\}$ is the conditional probability of losing the own vehicle in case of a MAC, which represents the quality of the Detect and Avoid (DAA) capability of the UAM aircraft.

4. Implementation and case study

To evaluate the first-party risk estimation methodology proposed in the previous section, we developed an interactive proof-of-concept web tool prototype built upon our previously developed interactive Quantitative Risk Assessment (QRA) platform for (third-party) air- and ground risk assessment [7, 8].

First, we implemented the algorithm for convex hull-based *LiU map* computation (Section 2), using population registry data for Norrköping Municipality, Sweden (Figure 3, left) as input to our prototype. The population density was aggregated onto a grid with 100x100m squares. We produced the convex hull-based LiU map, computing $m(g)$ for the squares of the input grid. Figure 3, right shows the resulting LiU map as a heatmap.

We further developed a web application [22] that enables users to interactively define a mission path and evaluate its risk KPIs in real time as the path is modified. In order to streamline risk management, the tool also provides a per-segment breakdown of risk KPIs, allowing users to identify high-risk portions of the route that would benefit from adjustment. The source code for both the convex hull-based *LiU map* computation and the interactive web tool is publicly available at [23].

4.1. Case study: Railway inspection

In order to evaluate our risk assessment methodology, we conducted a case study. In line with [6], we considered a railway inspection mission. We set the Near Mid Air Collision (NMAC)[5] distance to $2r = 152$ m, similarly to [6]. The average velocities of both the own vehicle and other drones were set at 30 km/h. We also consider the mitigation factor $\lambda_{\mathrm{STM}} = 1$, i.e., no DAA deconfliction is conducted. Essentially, we are studying the most conservative upper-bound, unmitigated, estimates to be able to assess what level of efficiency of conflict resolution capabilities is required for safe operation of manned urban aircraft. Finally, we assumed that there is only $n = 1$ person on board the railway inspection mission and that, on average, $N = 1$ other vehicle was flying during the mission. Since Formula 8 for EFR grows linearly with both N and n, our EFR estimates can trivially be scaled to other values of N and n.

Figure 5 shows the railway inspection route entered into our tool, which follows the railway that passes through Norrköping Central Station (Sweden). We assumed that the mission was conducted within the area of the Norrköping Municipality. Table 1 presents the corresponding per-segment breakdown of risk KPIs.

We observed a relatively high probability of encountering an NMAC with another drone. The standard target level of safety in UAM is in the order of one MAC per 10^6 flight hours [2], and our estimates for some mission segments were substantially above this value, even when taking into account the 1-to-100 ratio between MAC and NMAC. This demonstrates the importance of high-quality tactical DAA and strategic conflict resolution, as well as the potential need for more complex airspace structures, such as separating UAM vehicles across different altitude layers, in order to meet established aviation safety criteria.

The NMAC rate has varied almost 500-fold between the most dangerous (which go near the train station itself, which is close to the city center) and the least dangerous (in the unpopulated areas) parts of the mission. This high spatial variability of the risk further corroborates the need for route-specific risk assessments, such as ours, demonstrating that earlier assumptions for UAM that risk is spatially uniform may be inadequate.

In addition to that, the first-party risk KPIs were significantly higher than the corresponding air risk metrics, i.e., the risk posed by the own vehicle to conventional aviation, further highlighting the importance of first-party risk assessment for manned or passenger-carrying UAM operations.

[5] In [6], the MAC rate was derived by first calculating NMAC rate and then converting it into a MAC rate. In [24, 25] it was estimated as a result of Monte-Carlo simulations that the probability $p(\mathrm{MAC}|\mathrm{NMAC})$ of an NMAC resulting in a MAC is of the order of 10^{-2}. To stay comparable to [6], we followed the same approach by first calculating the NMAC and then converting it to MAC.

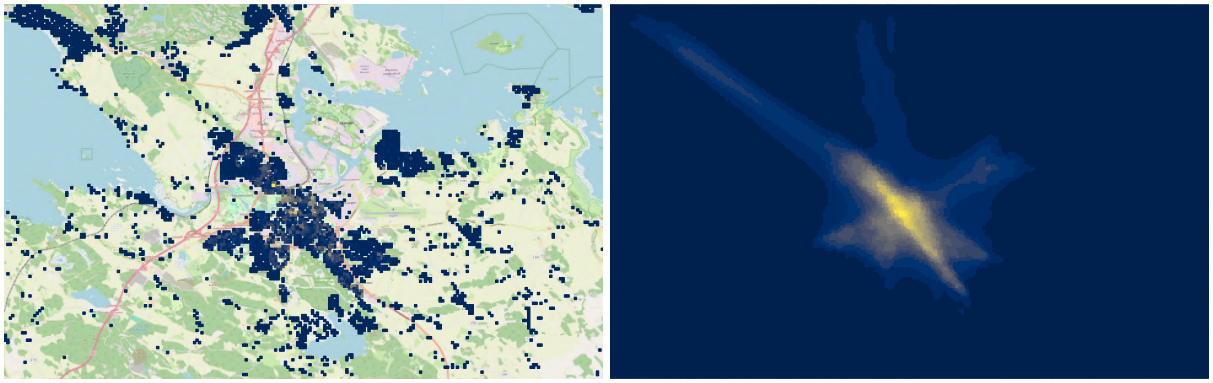

Fig. 3. *LiU map* for the area around Norrköping Municipality, Sweden. Left: Population density, with brighter colors indicating higher population; cells with zero population are omitted for clarity (data courtesy [21]). Right: Corresponding *LiU map*, where brighter colors indicate a higher probability of observing a drone).

Table 1. Per-segment breakdown of the safety KPIs of the railway inspection mission obtained from the risk assessment tool. The ground risk is computed based on the population density data (see Figure 3, left). The air risk is computed based on the anonymized general aviation flight tracks provided by Luftfartsverket (Swedish Civil Aviation Administration).

			Ground Risk				Air Risk		1st-Party Risk		
Seg.	Length (m)	Duration (min)	Exposed Pop. (ppl)	Affected area (m^2)	Avg. Exp. Pop. Density (ppl/m^2)	Max. Exp. Pop. Density (ppl/m^2)	NMAC / 10^6 flight hrs	NMAC of mission	NMAC / 10^6 flight hrs	NMAC of mission	EFR (/fh)
1–2	1437	3	6	319 148	$1.85 \cdot 10^{-5}$	$3.00 \cdot 10^{-4}$	0	0.00	942	$4.50 \cdot 10^{-5}$	$9.41 \cdot 10^{-4}$
2–3	2393	5	13	510 877	$2.46 \cdot 10^{-5}$	$4.00 \cdot 10^{-4}$	0	0.00	2814	$2.24 \cdot 10^{-4}$	$2.81 \cdot 10^{-3}$
3–4	1919	4	3	415 795	$5.79 \cdot 10^{-6}$	$3.00 \cdot 10^{-4}$	0	0.00	4866	$3.11 \cdot 10^{-4}$	$4.87 \cdot 10^{-3}$
4–5	2071	5	88	446 282	$1.96 \cdot 10^{-4}$	$2.50 \cdot 10^{-3}$	0	0.00	23 721	$1.64 \cdot 10^{-3}$	$2.37 \cdot 10^{-2}$
5–6	1133	3	0	258 373	0.00	0.00	33	$1.24 \cdot 10^{-6}$	34 834	$1.31 \cdot 10^{-3}$	$3.48 \cdot 10^{-2}$
6–7	1095	3	13	250 584	$5.17 \cdot 10^{-5}$	$6.00 \cdot 10^{-4}$	150	$5.45 \cdot 10^{-6}$	39 775	$1.45 \cdot 10^{-3}$	$3.98 \cdot 10^{-2}$
7–8	1164	3	83	264 565	$3.11 \cdot 10^{-4}$	$2.40 \cdot 10^{-3}$	99	$3.84 \cdot 10^{-6}$	93 998	$3.64 \cdot 10^{-3}$	$9.40 \cdot 10^{-2}$
8–9	1134	3	310	258 490	$1.20 \cdot 10^{-3}$	$3.70 \cdot 10^{-3}$	124	$4.65 \cdot 10^{-6}$	126 499	$4.78 \cdot 10^{-3}$	$1.26 \cdot 10^{-1}$
9–10	810	2	188	193 588	$9.67 \cdot 10^{-4}$	$1.53 \cdot 10^{-2}$	136	$3.67 \cdot 10^{-6}$	78 086	$2.11 \cdot 10^{-3}$	$7.81 \cdot 10^{-2}$
10–11	795	2	376	190 591	$1.97 \cdot 10^{-3}$	$1.21 \cdot 10^{-2}$	162	$4.26 \cdot 10^{-6}$	162 377	$4.30 \cdot 10^{-3}$	$1.62 \cdot 10^{-1}$
11–12	676	2	762	166 646	$4.57 \cdot 10^{-3}$	$2.62 \cdot 10^{-2}$	384	$8.62 \cdot 10^{-6}$	482 888	$1.09 \cdot 10^{-2}$	$4.83 \cdot 10^{-1}$
12–13	680	2	246	167 391	$1.47 \cdot 10^{-3}$	$2.62 \cdot 10^{-2}$	356	$8.05 \cdot 10^{-6}$	470 893	$1.06 \cdot 10^{-2}$	$4.71 \cdot 10^{-1}$
13–14	773	2	3	186 116	$1.53 \cdot 10^{-5}$	$3.00 \cdot 10^{-4}$	339	$8.70 \cdot 10^{-6}$	148 071	$3.81 \cdot 10^{-3}$	$1.48 \cdot 10^{-1}$
14–15	1190	3	0	269 743	0.00	0.00	462	$1.83 \cdot 10^{-5}$	89 516	$3.55 \cdot 10^{-3}$	$8.95 \cdot 10^{-2}$
15–16	1126	3	2	256 919	$7.66 \cdot 10^{-6}$	$4.00 \cdot 10^{-4}$	186	$6.96 \cdot 10^{-6}$	69 352	$2.60 \cdot 10^{-3}$	$6.94 \cdot 10^{-2}$
16–17	1128	3	45	257 259	$1.74 \cdot 10^{-4}$	$2.70 \cdot 10^{-3}$	51	$1.88 \cdot 10^{-6}$	78 735	$2.96 \cdot 10^{-3}$	$7.87 \cdot 10^{-2}$
17–18	896	2	15	210 709	$6.83 \cdot 10^{-5}$	$2.70 \cdot 10^{-3}$	55	$1.63 \cdot 10^{-6}$	68 741	$2.05 \cdot 10^{-3}$	$6.87 \cdot 10^{-2}$
18–19	1031	3	21	237 814	$8.43 \cdot 10^{-5}$	$1.40 \cdot 10^{-3}$	13	$4.26 \cdot 10^{-7}$	55 060	$1.89 \cdot 10^{-3}$	$5.51 \cdot 10^{-2}$
19–20	1062	3	10	244 096	$3.86 \cdot 10^{-5}$	$9.00 \cdot 10^{-4}$	404	$1.43 \cdot 10^{-5}$	48 502	$1.71 \cdot 10^{-3}$	$4.85 \cdot 10^{-2}$

5. Conclusions and future work

We presented a quantitative methodology for high-fidelity first-party risk estimation for UAM; we also developed a proof-of-concept implementation to demonstrate its applicability. The proposed approach enables both airspace users and regulatory authorities to assess mission-specific risks in a detailed and interactive manner.

The conducted railway inspection case study demonstrated that first-party risks can become substantial even under low-density traffic assumptions. In particular, the estimated probabilities of NMAC and MAC for some mission segments exceeded established aviation safety targets by a considerable margin. Furthermore, the results showed that risk levels may vary significantly along a mission route, highlighting the importance of segment-level and route-specific risk assessment approaches for first-party risks.

As the volume of UAM operations increases, the frequency of conflicts between the vehicles is expected to rise. This highlights the growing importance of incorporating Detect and Avoid (DAA) capabilities into both operational systems and risk assessment methodologies. Future work will focus on integrating DAA performance models into the proposed framework, as well as extending the methodology to account for more complex traffic patterns and airspace structures. In addition, the incorporation of restricted areas (geofences) into the model represents an important direction for further research. Because operators typically prefer to fly along the shortest routes, the introduction of restricted areas may cause drone trajectories to concentrate along the boundaries of such regions. This may lead to increased conflict rates near the edges, as well as local congestion, elevated noise levels, and greater visual pollution. These effects could be mitigated by enforcing route planning strategies that maintain sufficient clearance from obstacles, for

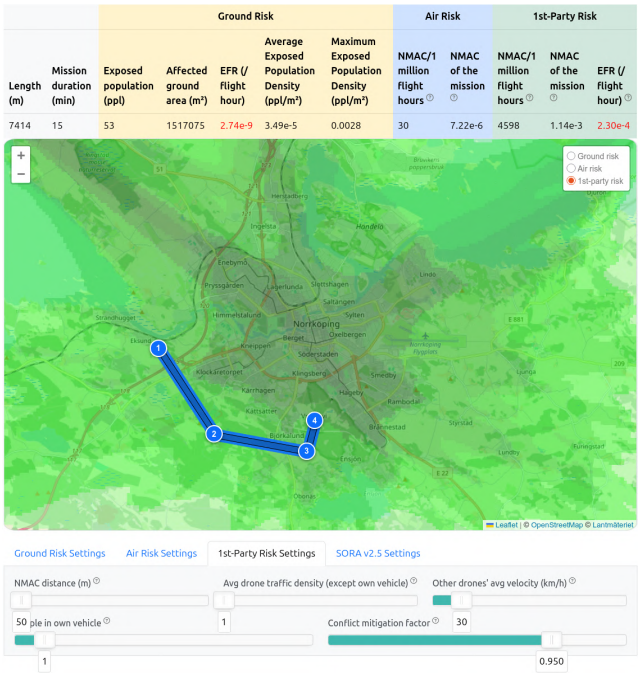

Fig. 4. Interactive real-time risk assessment web tool prototype which implements our proposed first-party risk assessment methodology. The first-party risk KPIs are displayed in the top-right corner. Key parameters, including the MAC separation distance, N, the average velocity of other drones, the number of people in the own vehicle, and the conflict mitigation factor λ_{STM} can be adjusted via sliders in the bottom panel. The blue lines indicate the mission route, while the underlying green map represents the drone map shown in Figure 3. The tool is available at [22], and the source code is provided at [23].

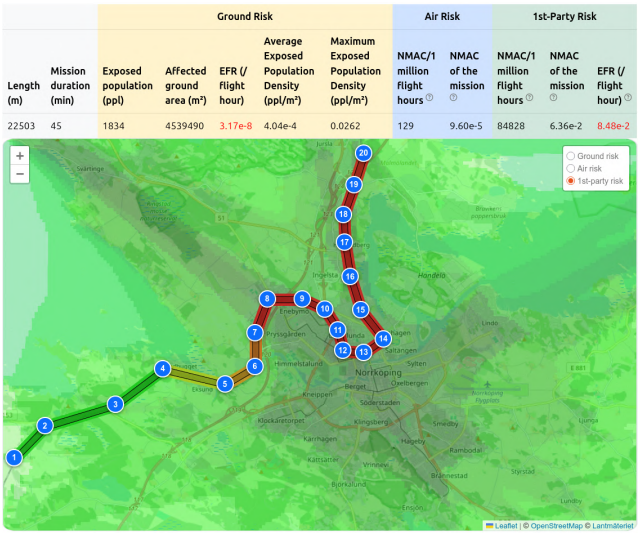

Fig. 5. Railway inspection mission entered in the risk assessment tool. Colors of the route segments represent the relative 1st-party risk (green is the lowest risk, dark-red is the highest risk). The per-segment breakdown of risk KPIs is presented in Table 1.

example, by requiring paths to remain well separated from restricted areas [26, 27, 28] or by employing medial-axis routing [29, 30]. Investigating these approaches within the proposed framework is left for future work.

In addition to that, more realistic demand distribution models and scenarios would significantly improve the quality of the drone probability map. Our experiments focused on population density-based demand model, but in reality there will likely be some "demand hotspots" such as police stations, hospitals, stores, restaurants with takeout delivery, from and to which flights will be originating and arriving. Such major sources of demand may significantly shift the spatial probability map picture, creating dangerous high-traffic "corridors" where drones will be often flying (especially in the presence of restricted zones). In addition to that, our population density is static, i.e., we used the population registry of where people sleep. In reality, population significantly shifts during different parts of day, moving between suburban areas and the city center packed with office buildings. We leave to future work development of such realistic dynamic spatial demand models.

6. Acknowledgments

The work of LS and VP is partially supported by the Swedish Transport Administration (Trafikverket). The work of MW is partially supported by the Staff Mobility for Training (STT) under the Swiss-European Mobility Program (SEMP).

LS and VP thank Mikael Henriksson (Digital Tower Consulting) and Billy Josefsson (LiU) for consultations.

References

1) European Union Aviation Safety Agency, "Study on the societal acceptance of urban air mobility in Europe," European Union Aviation Safety Agency, Cologne, Germany, Tech. Rep., 2021. [Online]. Available: https://www.easa.europa.eu/en/downloads/127760/en

2) JARUS, "JARUS guidelines on specific operations risk assessment (SORA), Edition 2.5," May 2024, sORA v2.5 Main Body Release. [Online]. Available: http://jarus-rpas.org/publications/

3) P. J. van der Geest, Y. S. Cheung, and T. M. van Birgelen, "Safety targets for UAM vehicles," 2021.

4) J. Stjernberg, P. Durnford, P. van Egmond, J. Krivohlavek, R. Martijnse-Hartikka, S. A. Solbø, F. Wachter, and K. Wigler, "Guidebook for urban air mobility integration," AiRMOUR Project (EU Horizon 2020), Project Deliverable Deliverable 6.4, 2023, funded by the European Union's Horizon 2020 research and innovation programme under grant agreement No 101006601. [Online]. Available: https://airmour.eu/deliverables/

5) A. la Cour-Harbo and H. Schiøler, "Probability of low-altitude midair collision between general aviation and unmanned aircraft," *Risk Analysis*, vol. 39, no. 11, pp. 2499–2513, Nov. 2019. [Online]. Available: https://doi.org/10.1111/risa.13368

6) X. Olive, P. Le Blaye, L. Sedov, and T. Krauth, "Quantitative air risk assessment for a drone inspection mission along fast-train lines," in *Proceedings of the 15th ATM Seminar 2023, Savannah, Georgia, United States of America, June 5-9, 2023*, 2023.

7) L. Sedov, V. Polishchuk, T. Maury, M. Ulloa, and D. Lykova, "Qualitative and quantitative risk assessment of urban airspace operations,"

Proceedings of the SESAR Innovation Days (SID 2021), Virtually, pp. 7–9, 2021.

8) L. Sedov, V. Polishchuk, and V. Bulusu, "Ground risk vs. efficiency in urban drone operations," in *Proceedings of the 14th ATM Seminar*, vol. 21, 2021.

9) ——, "Sampling-based capacity estimation for unmanned traffic management," in *Proceedings of the 2017 IEEE/AIAA 36th Digital Avionics Systems Conference (DASC)*. IEEE, 2017, pp. 1–10.

10) E. Sunil, J. Hoekstra, J. Ellerbroek, F. Bussink, D. Nieuwenhuisen, A. Vidosavljevic, and S. Kern, "Metropolis: Relating airspace structure and capacity for extreme traffic densities," in *Proceedings of the ATM Seminar 2015, 11th USA/EUROPE Air Traffic Management R&D Seminar*, 2015.

11) N. Patrinopoulou, I. Daramouskas, V. Lappas, V. Kostopoulos, A. Morfin Veytia, C. A. Badea, J. Ellerbroek, J. Hoekstra, P. Menendez, P. Alonso, J. Gonzalez, D. Bereziat, A. Vidosavljevic, and L. Sedov, "Metropolis ii: Investigating the future shape of air traffic control in highly dense urban airspace," in *Proceedings of the 30th Mediteranean Conference on Control and Automation*, 07 2022.

12) L. Sedov and V. Polishchuk, "Centralized and distributed UTM in layered airspace," in *Proceedings of the 8th International Conference on Research in Air Transportation*, 2018, pp. 1–8.

13) L. Sedov, V. Polishchuk, and V. Bulusu, "Sampling-based capacity estimation for unmanned traffic management," in *Proceedings of the 2017 IEEE/AIAA 36th Digital Avionics Systems Conference (DASC)*. IEEE, 2017, pp. 1–10.

14) V. Bulusu and V. Polishchuk, "A threshold based airspace capacity estimation method for UAS traffic management," in *Proceedings of the 2017 Annual IEEE International Systems Conference (SysCon)*. IEEE, 2017, pp. 1–7.

15) L. C. Freeman, "A set of measures of centrality based on betweenness," *Sociometry*, pp. 35–41, 1977.

16) L. Popa, A. Rostamizadeh, R. Karp, C. Papadimitriou, and I. Stoica, "Balancing traffic load in wireless networks with curveball routing," in *Proceedings of the 8th ACM International Symposium on Mobile Ad Hoc Networking and Computing*, 2007, pp. 170–179.

17) B. I. Schuchardt, A. Andreeva-Mori, P. H. Kopardekar, V. Kramar, J. Murphy, M. Condé Rocha Murça, and D. Sziroczák, "Scientific assessment for urban air mobility (uam)," *CEAS Aeronautical Journal*, pp. 1–36, 2026.

18) European Union Aviation Safety Agency (EASA), "Frequently asked questions on urban air mobility (UAM)," https://www.easa.europa.eu/sites/default/files/dfu/uam_-_faqs.pdf, 2021, accessed: 2026-04-20.

19) R. Storvold, C. Sweatte, P. Ruel, M. Wuennenberg, K. Tarr, M. Raustein, T. Hillesøy, T. Lundgren, and M. Sumich, "Arctic science RPAS operator's handbook," Arctic Monitoring and Assessment Programme (AMAP), Tech. Rep., 2015.

20) R. E. Weibel and R. J. Hansman, "Safety considerations for operation of unmanned aerial vehicles in the National Airspace System," MIT, Tech. Rep., 2006.

21) Swedish University of Agricultural Sciences, "Population density data source," http://www.slu.se/en/.

22) H. Hasan, L. Sedov, S. Carlswärd, and V. Polishchuk, "UAV quantitative risk assessment tool," https://undefiened.github.io/uav_risk/, 2026, flight Logistics Unit, Linköping University.

23) L. Sedov, "Quantitative risk assessment tool prototype source code," https://github.com/undefiened/QRA_tool, 2026.

24) M. Kochenderfer, D. Griffith, and J. Olszta, "On estimating mid-air collision risk," in *10th AIAA Aviation Technology, Integration, and Operations (ATIO) Conference*, 2010. [Online]. Available: https://doi.org/10.2514/6.2010-9333

25) A. Weinert, S. Campbell, A. Vela, D. Schuldt, and J. Kurucar, "Well-clear recommendation for small unmanned aircraft systems based on unmitigated collision risk," *Journal of Air Transportation*, vol. 26, no. 3, pp. 113–122, 2018. [Online]. Available: https://doi.org/10.2514/1.D0091

26) V. Polishchuk and J. S. Mitchell, "Thick non-crossing paths and minimum-cost flows in polygonal domains," in *Proceedings of the 23rd Annual Symposium on Computational Geometry*, 2007, pp. 56–65.

27) E. M. Arkin, J. S. Mitchell, and V. Polishchuk, "Maximum thick paths in static and dynamic environments," in *Proceedings of the 24th Annual Symposium on Computational Geometry*, 2008, pp. 20–27.

28) S. Yang, J. S. Mitchell, J. Kim, J. Zou, J. Krozel, and V. Polishchuk, "Flexible airlane generation to maximize flow under hard and soft constraints," *Air Traffic Control Quarterly*, vol. 19, no. 3, pp. 211–235, 2011.

29) J. Gao and M. Goswami, "Medial axis based routing has constant load balancing factor," in *Proceedings of the Algorithms-ESA 2015: 23rd Annual European Symposium, Patras, Greece, September 14-16*. Springer, 2015, pp. 557–569.

30) J. Bruck, J. Gao, and A. Jiang, "Map: Medial axis based geometric routing in sensor networks," in *Proceedings of the 11th annual international conference on Mobile computing and networking*, 2005, pp. 88–102.